This is an open access article published under a Creative Commons Attribution (CC-BY) License, which permits unrestricted use, distribution and reproduction in any medium, provided the author and source are cited.

JACS JOURNAL OF THE AMERICAN CHEMICAL SOCIETY

Article

Cite This: J. Am. Chem. Soc. 2019, 141, 8264−8276

pubs.acs.org/JACS

Mechanism of Olefin Metathesis with Neutral and Cationic Molybdenum Imido Alkylidene *N*-Heterocyclic Carbene Complexes

Katharina Herz,[§] Maren Podewitz,*[,†] Laura Stöhr,[§] Dongren Wang,[§] Wolfgang Frey,[‡] Klaus R. Liedl,[†] Suman Sen,[§] and Michael R. Buchmeiser*[,§]

[§]Institute of Polymer Chemistry and [‡]Institute of Organic Chemistry, University of Stuttgart, Pfaffenwaldring 55, D-70569 Stuttgart, Germany

[†]Institute of General, Inorganic and Theoretical Chemistry, University of Innsbruck, Innrain 80-82, A-6020 Innsbruck, Austria

Supporting Information

ABSTRACT: A series of neutral molybdenum imido alkylidene *N*-heterocyclic carbene (NHC) bistriflate and monotriflate monoalkoxide complexes as well as cationic molybdenum imido alkylidene triflate complexes have been subjected to NMR spectroscopic, X-ray crystallographic, and reaction kinetic measurements in order to gain a comprehensive understanding about the underlying mechanism in olefin metathesis of this new type of catalysts. On the basis of experimental evidence and on DFT calculations (BP86/def2-TZVP/D3/cosmo) for the entire mechanism, olefinic substrates coordinate trans to the NHC of neutral 16-electron complexes via an associative mechanism, followed by dissociation of an anionic ligand (e.g., triflate) and formation of an intermediary molybdacyclobutane trans to the NHC. Formation of a cationic complex is crucial in order to become olefin metathesis active. Variations in the NHC, the imido, the alkoxide, and the noncoordinating anion revealed their influence on reactivity. The reaction of neutral 16-electron complexes with 2-methoxystyrene is faster for catalysts bearing one triflate and one fluorinated alkoxide than for catalysts bearing two triflate ligands. This is also reflected by the Gibbs free energy values for the transition states, $\Delta G^{\ddagger}_{303}$, which are significantly lower for catalysts bearing only one triflate than for the corresponding bistriflate complexes. Reaction of a solvent-stabilized cationic molybdenum imido alkylidene *N*-heterocyclic carbene (NHC) monotriflate complex with 2-methoxystyrene proceeded via an associative mechanism too. Reaction rates of both solvent-free and solvent-stabilized cationic Mo imido alkylidene NHC catalysts with 2-methoxystyrene are controlled by the cross-metathesis step but not by adduct formation.

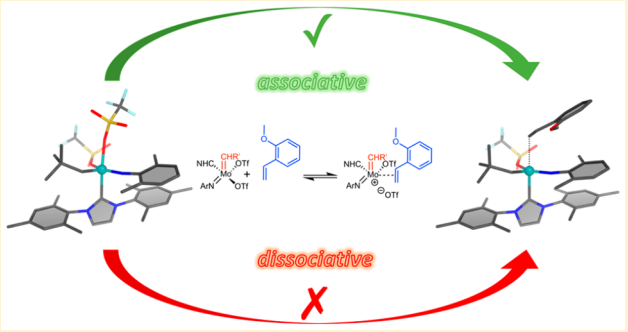

INTRODUCTION

Olefin metathesis with well-defined metal alkylidenes has long been dominated by Schrock- and Grubbs-type catalysts,[1−7] mostly because of their most favorable properties in terms of regio-, chemo-, and stereoselectivity[8−22] and often specificity in many olefin metathesis reactions including those related to polymer chemistry.[23−25] Aiming at ionic olefin metathesis catalysts for use in biphasic reactions, we recently reported on a new class of neutral and cationic molybdenum imido, tungsten imido, and tungsten oxo alkylidene *N*-heterocyclic carbene (NHC) complexes as a new family of group 6 olefin metathesis catalysts and successfully carried out substantial variations in both the imido and the NHC ligand.[26−35] While molybdenum imido alkylidene NHC bistriflate complexes display substantial activity and functional group tolerance both in the cyclopolymerization of α,ω-diynes and in ring-opening metathesis polymerization (ROMP), particularly cationic molybdenum imido, tungsten imido, and tungsten oxo alkylidene NHC complexes and their silica-supported versions show high activity and productivity in ring-closing metathesis (RCM), cross-metathesis (CM), and homometathesis (HM), reaching turnover numbers > 1 200 000.[27,36,37] We found that molybdenum imido alkylidene NHC bistriflate complexes possess a coalescence temperature, T_c, for the two triflates and that there is a correlation between T_c and both productivity and activity at a given temperature.[27,33] Further important findings were that neutral complexes containing at least one triflate are activated by the release of triflate. The propensity of the precatalyst to form an olefin metathesis-active, cationic species strongly depends on the imido ligand, the nature of the second anionic ligand, the σ-donor propensity of the NHC used, and the spatial arrangement of the ligands.[27,33] Further stabilization is achieved by introduction of a second, chelating ligand and allows for the synthesis of air-stable 18-electron progenitors. In the case of molybdenum imido alkylidene NHC bistriflate complexes, this particular feature has been used to create fully room-temperature-latent precatalysts, e.g., for the ROMP of dicyclopentadiene (DCPD).[38,39] In view of the discovery that dissociation of one triflate ligand from a neutral 16-electron

Received: February 23, 2019
Published: April 27, 2019

© 2019 American Chemical Society

DOI: 10.1021/jacs.9b02092
J. Am. Chem. Soc. 2019, 141, 8264−8276

complex is a crucial step, we started a detailed mechanistic study on the reaction mechanism using complexes **1**−**10** as representatives of neutral Mo imido alkylidene NHC bistriflate and monotriflate monoalkoxide and cationic Mo imido alkylidene triflate complexes (Chart 1). Experimental investigations were corroborated by extensive DFT studies of the entire reaction mechanism. Here we report our results.

Chart 1. Structure of Catalysts 1−13[a]

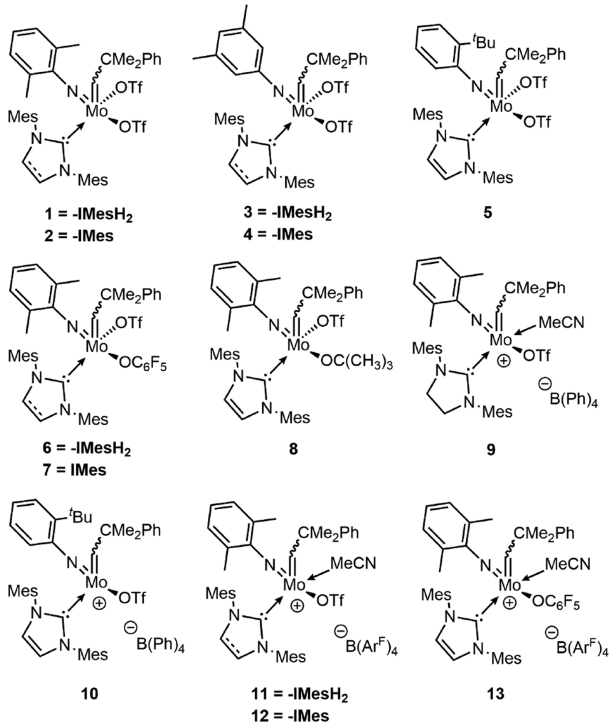

[a]Mes = 2,4,6-$(CH_3)_3C_6H_2$, OTf = CF_3SO_3, $B(Ar^F)_4$ = B(3,5-$(CF_3)_2$-$C_6H_3)_4$.

RESULTS AND DISCUSSION

Coalescence Temperatures of Neutral 16-Electron Mo Imido Alkylidene NHC (OTf)(OR) Complexes (R = Tf, alkyl, aryl). On the basis of the observation that bis(triflate) complexes show a coalescence temperature for the two triflate groups, an activation mechanism based on a Berry-type pseudorotation, i.e., interconversion between trigonal biyramidal (TBP) configuration through a square pyramidal (SP) configuration, was proposed. Activation of the catalysts through the release of one triflate (thermally induced) in the SP configuration is in full accordance with the observed reactivity of both neutral and cationic Mo−imido alkylidene NHC complexes and with ^{19}F NMR.[40] In principle, an olefin metathesis reaction starting from neutral, pentacoordinated 16-electron Mo/W imido or oxo alkylidene NHC complexes can occur in a *dissociative* fashion, with one triflate leaving the complex, thereby generating a cationic 14-electron species, followed by coordination of substrate. Alternatively, the reaction can proceed in an *associative* fashion where substrate coordination is followed by the dissociation of triflate (Scheme 1). In principle, depending on the reaction mechanism, the individual steps can be described by a series of rate constants, k_1, k_{-1}, k_1', k_{-1}', etc. These, however, cannot be assessed individually by experiment but eventually by quantum chemical investigations. To render the overall reaction irreversible, we chose the reaction of complexes **1**−**10** with excess (10 equiv) 2-methoxystyrene. This particular set of catalysts was selected because it represents a variety of modifications in the imido, alkoxide, and NHC ligand. In fact, complexes **1**−**10** undergo quantitative and irreversible CM reaction. In the case of the pentacoordinated starting compounds, octahedral complexes are formed, which are all stabilized by the coordination of oxygen (Scheme 1). To the best of our knowledge, the observation of olefin adducts for other molybdenum metathesis-based catalysts has not been stated so far. Indeed, it was proposed that in solvent-containing Mo-based Schrock catalysts the solvent first has to dissociate from the complex prior to olefin coordination.[41,42]

Complex **2a** (Figure 1) served as representative example and is formed via the reaction of **2** with 2-methoxystyrene in quantitative yield. It crystallizes in the orthorhombic space group $Pna2_1$, a = 1910.70(14) pm, b = 1214.69(8) pm, c = 1739.38(11) pm, $\alpha = \beta = \gamma = 90°$, Z = 4, which is a chiral space group and contains both enantiomers. Relevant bond lengths and angles are summarized in Figure 1.

In the solid state, **2a** adopts a distorted octahedral (O_h) configuration in which the alkylidene is in the anti configuration, also visible in the coupling constant of the satellites in ^1H NMR ($^1J_{CH}$ = 150 Hz)[43] and in line with the DFT-optimized structure. The methoxy group is coordinating trans to the imido ligand (161.49°) with a comparably long Mo−O distance (Mo(1)−O(7) = 243.7(2) pm). The bond lengths of the Mo−triflates are comparable to those in complexes **1** and **2**.[27] The analogous

Scheme 1. Possible Reaction Mechanisms with Mo−Imido Alkylidene NHC Complexes

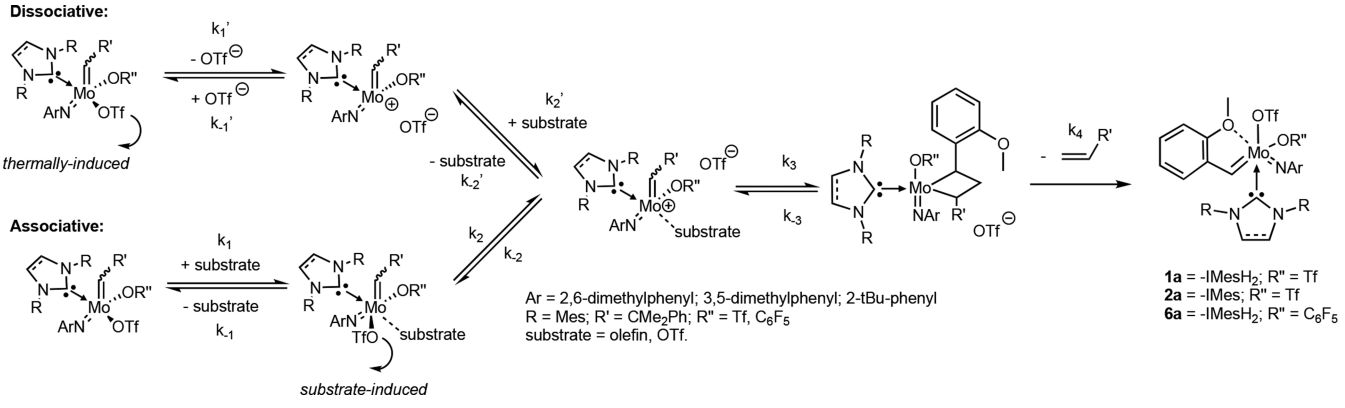

DOI: 10.1021/jacs.9b02092
J. Am. Chem. Soc. 2019, 141, 8264−8276

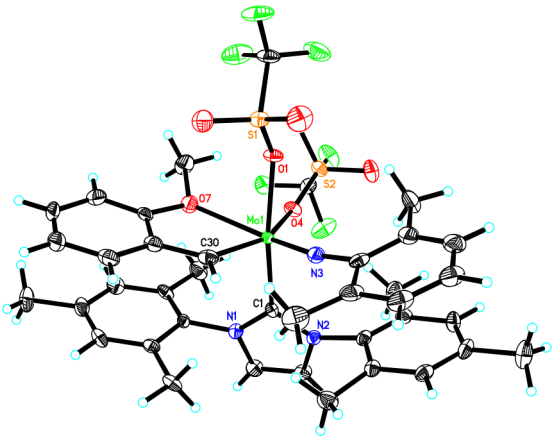

Figure 1. Single-crystal X-ray structure of **2a**. Relevant bond lengths (pm) and angles (deg): Mo(1)−N(3) 171.4(2), Mo(1)−C(34) 196.4(3), Mo(1)−O(4) 221.0(2), Mo(1)−O(1) 213.73(18), Mo(1)−C(1) 222.1(3), Mo(1)−O(7) 243.7(2), N(3)−Mo(1)−C(30) 93.70(14), N(3)−Mo(1)−O(1) 94.17(9), N(3)−Mo(1)−O(7) 161.49(11), C(30)−Mo(1)−O(1) 100.58(10), N(3)−Mo(1)−O(4) 117.01(12), C(30)−Mo(1)−O(4) 149.29(11), O(4)−Mo(1)−O(1) 78.74(7), N(3)−Mo(1)−C(1) 94.62(11), C(30)−Mo(1)−C(1) 97.53(12), O(4)−Mo(1)−C(1) 80.55(9), O(1)−Mo(1)−C(1) 159.28(9).

complex **6a** is formed via the reaction of **6** with 2-methoxystyrene in 87% isolated yield (Figure S101, SI). The coalescence temperatures, T_c, for the two triflates in the bistriflate complexes **1**, **2**, and **5** were measured via ^{19}F NMR in 1,2-dichlorobenzene-d_4; those of complexes **3** and **4** were measured in dichloromethane-d_2. The T_c of the monotriflate complexes **6**−**8** was determined by adding 1 equiv of tetrabutylammonium triflate (TBAT) with respect to the catalyst to a solution of the corresponding catalyst in 1,2-dichlorobenzene-d_4. Depending on the structure, the T_c values varied between −30 and 100 °C. Notably, addition of 1 equiv of TBAT to **1** in 1,2-dichlorobenzene-d_4 revealed a second T_c at 90 °C. This finding clearly illustrates distinct differences between a thermally induced triflate dissociation and a substrate-induced triflate dissociation, referred to as "associative", both outlined in Scheme 1. In fact, additional triflate or any nucleophile or olefin has been already proposed to interact by coordinating first trans to the NHC followed by dissociation of triflate and ligand rearrangement.[27,32,33] This is in line with calculations on tetracoordinated 14-electron Schrock catalysts, which also propose a trans approach of substrate to the strongest σ-donor.[44,45] In the case of pentacoordinated 16-electron complexes discussed here, addition of triflate is proposed to yield (intermediary) anionic complexes, which was deemed reasonable since such an anionic complex was found to be stable in a DFT structure optimization (Figure S134, SI). In view of the dianionic W imido alkylidene *N*-heterocyclic olefin (NHO)[46] and anionic molybdenum imido alkylidene bisamido monotriflate complexes reported earlier,[31] such an anionic intermediate seems viable. For spectroscopic evidence for this proposal, see the Supporting Information.

Compound **8**, obtained via the reaction of **2** with 1 equiv of Li *tert*-butoxide, has a T_c in the presence of TBAT below −60 °C. An accurate value could not be detected due to technical limitations in cooling. Accordingly, in the ^{19}F NMR spectrum of **8** recorded at 25 °C the triflate signal at δ = −78.97 ppm points toward a cationic metal center. However, complex **8** showed no reactivity for 2-methoxystyrene at all, even at 90 °C. This is at a first glance contradictory since at 90 °C **8** must be cationic with virtually no bonding of triflate to the metal center. However, its metathetical inactivity can be attributed to a stabilization of the positive charge at the cationic metal center by both the *tert*-butoxide and the NHC ligand (Figure S7, SI). This stabilization substantially reduces the electrophilic character of the cationic metal center and is in turn also responsible for OTf dissociation even at very low temperature. Similar results have already been reported for, e.g., cationic tungsten imido alkylidene NHC complexes;[30] all together, they illustrate the effectiveness of charge stabilization by the NHC and an electron-donating alkoxide. On a final note, it should also be mentioned that the T_c of **4** in toluene-d_8 is 60 °C and thus 90 °C higher than that in CH_2Cl_2 (T_c = −30 °C).[2] This pronounced dependence of T_c on the polarity of the solvent further supports the involvement of highly polar if not ionic intermediates and/or transition states.

From the T_c values one can estimate the Gibbs free activation energy, $\Delta G^{\ddagger}_{Tc}$, for the underlying process. Thus, the rate constant, k_c, of the dynamic exchange at T_c was estimated according to eq 1, where $\Delta\vartheta$ is the difference in resonance frequencies determined in the slow exchange limit, N_A is Avogadro's constant, and h is Planck's constant. Applying eq 2,[47] $\Delta G^{\ddagger}_{Tc}$ was calculated.

$$k_c = \frac{\pi}{\sqrt{2}}\Delta\vartheta \tag{1}$$

$$\Delta G^{\ddagger}_{T_c} = RT_c \cdot \ln\frac{RT_c\sqrt{2}}{\pi \cdot N_A \cdot h\Delta\vartheta} \tag{2}$$

$\Delta G^{\ddagger}_{Tc}$ values of the bistriflate and monotriflate monophenoxide complexes **1**−**7** were in the range of 46−69 kJ·mol^{-1}. The lowest values were found for **3** and **4** based on the 3,5-dimethylphenylimido ligand. By contrast, the $\Delta G^{\ddagger}_{Tc}$ values were not strongly influenced by the nature of the anionic ligands, i.e., triflate vs pentafluorophenoxide. This points toward steric rather than electronic effects on T_c and in due consequence on $\Delta G^{\ddagger}_{Tc}$; nonetheless, in order to come up with a comprehensive picture, further investigations need to be carried out on that issue.

Reaction Kinetics. Reactions of catalysts **1**−**10** with 2-methoxystyrene were followed by ^{1}H NMR spectroscopy at 30 °C.[48] Quantification of the reaction kinetics of the cationic complexes **11** and **13** based on the $B(Ar^F)_4^-$ anion was initially hampered by the formation of polymer. In line with ^{1}H NMR experiments, which showed that a mixture of tris(pentafluorophenyl)borane or anilinium tetrakis(3,5-bis(trifluoromethyl)phenyl)borate with 2-methoxystyrene produced polymer (Figure S70, SI), reactions of catalysts **11**−**13** containing the $B(Ar^F)_4^-$ anion (Chart 1) with 2-methoxystyrene predominantly also induced the polymerization of 2-methoxystyrene, attributable to a cationic polymerization of a phenylogous vinyl ether. However, ^{1}H NMR measurements with $NaBPh_4$ and 2-methoxystyrene revealed no polymerization within 8 h. We therefore synthesized the acetonitrile-containing cationic complex **9** containing tetraphenylborate[49−52] as counteranion and successfully monitored its reaction with 2-methoxystyrene.

In situ ^{1}H and ^{19}F NMR spectroscopy on the reaction of **1** with 3 equiv of 2-methoxystyrene revealed formation of an adduct, which was then converted into the final 18-electron complex. In the case where the reaction was carried out at 30 °C in CD_2Cl_2, broad signals for both triflates at δ = −75.67 and

DOI: 10.1021/jacs.9b02092
J. Am. Chem. Soc. 2019, 141, 8264−8276

−77.58 ppm were observed in the ^{19}F NMR spectra (Figure S10, SI). By comparing the relative ratios of these signals with those of the alkylidene signals of **1** and the product, **1a**, in ^{1}H NMR (Figure S9, SI), these signals can be clearly assigned to an adduct that contains two triflates *and* coordinated 2-methoxystyrene (Scheme 1, Figure 2), which was corroborated by DFT calculations, where such a stable neutral adduct was localized for **2** (vide infra). Notably, such an associate mechanism is in stark contrast to the dissociate pathway that was proposed for solvent-stabilized 16-electron Schrock catalysts, for which tetracoordinate, solvent-free species were proposed to represent the active species.[41,42] The structure of this adduct was further confirmed by signals in the ^{1}H NMR at δ = 8.23 ppm for the H_α of the benzylic proton in 2-methoxystyrene and at δ = 6.69 ppm, which show the terminal olefinic protons of 2-methoxystyrene in the 16-electron complex (Figure S9, SI). In the ^{19}F NMR spectrum, next to the product signals at δ = −76.91 and −78.54 ppm, additionally free triflate was observed at −79.06 ppm (Figure S12, SI). In view of the peak half widths of all signals (Figure S10, SI), a fast triflate exchange can be accounted for the adduct but neither for **1** nor for the product. This rapid triflate exchange was observed for complexes **1**−**7**, **9**, and **10** with 2-methoxystyrene and points toward a cationic species.

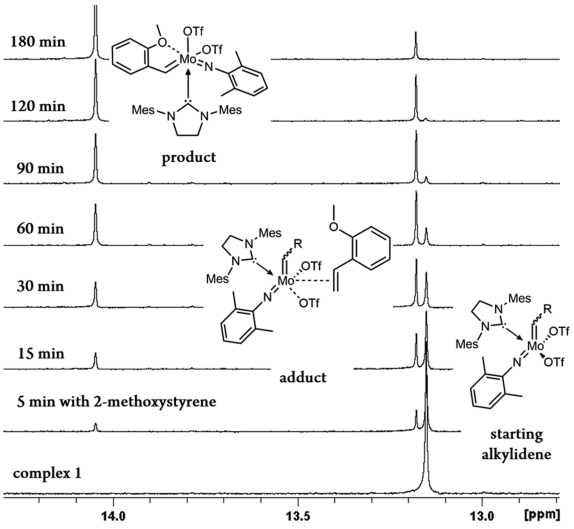

Figure 2. ^{1}H NMR spectrum (alkylidene region) of the reaction of catalyst **1** with 2-methoxystyrene (1,2-dichloroethane-d_4).

DFT calculations support this finding. Thus, a very low barrier was found for the dissociation of triflate in **2** ($\Delta E_{rel}^{\ddagger}$ = 12.9 kJ·mol^{-1}/$\Delta G_{rel}^{\ddagger}$ = 5.9 kJ·mol^{-1}). All adducts were reactive but sufficiently stable, so their conversion into the final 18-electron complex could be followed by ^{1}H NMR. Scheme 2 illustrates the simplified reaction scheme of the starting complex with 2-methoxystyrene including adduct and product formation. Instead of the rate constants k_1, k_{-1}, k_2, k_{-2}, k_3, k_{-3}, and k_4, which cannot be assessed individually, the overall rate constants k_a (rate constant for olefin coordination) and k_b (rate constant

Scheme 2. Associative Reaction Mechanism of Bistriflate, Monoalkoxide Monotriflate (top), Cationic Catalyst with Stabilizing Solvent (middle), and Cationic Catalyst without Stabilizing Solvent (bottom)[a]

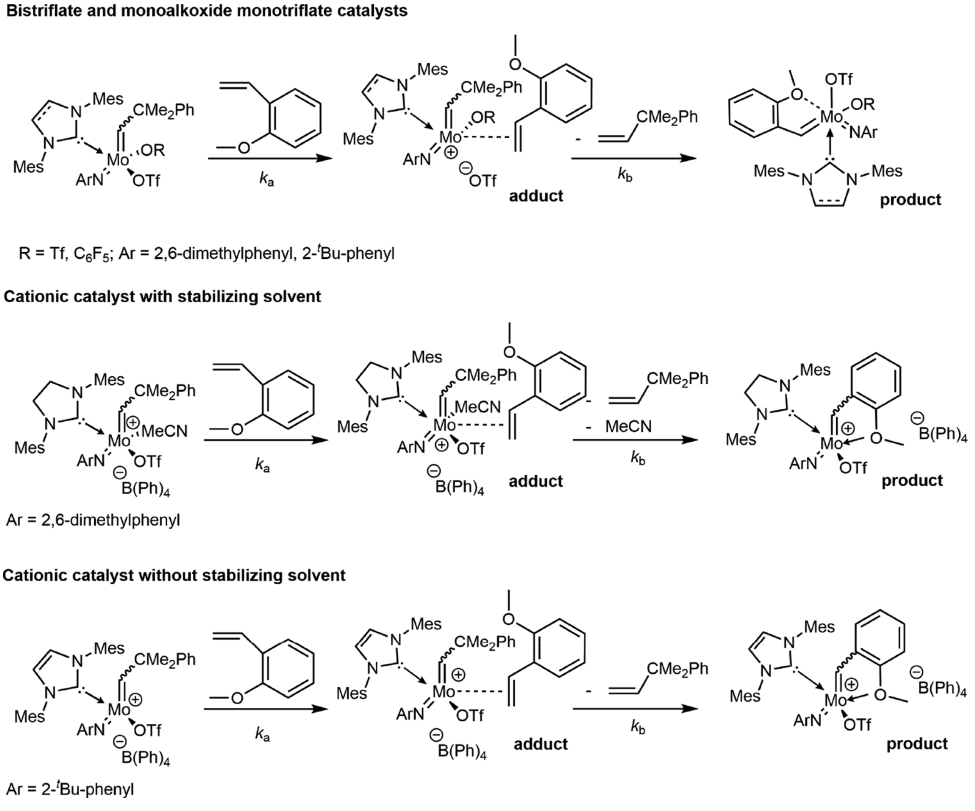

[a]Indeed, DFT calculations predicted a very stable adduct (Figure S.131, SI) (vide infra). In line with that, the rate constants for the *solvent-free* catalyst **10** could not be determined at 30 °C due to a very fast reaction with 2-methoxystyrene. However, low-temperature measurements carried out at −10 °C showed a reaction rate of 1.0 L·mol$^{-1.}$ min^{-1} as well as the lowest Gibbs free activation energy for adduct formation of all complexes examined here ($\Delta G^{\ddagger}_{303}$ = 69.5 kJ·mol^{-1}), which reflects the high reactivity of this compound in CM.

DOI: 10.1021/jacs.9b02092
J. Am. Chem. Soc. 2019, 141, 8264−8276

for cross metathesis) can be estimated (Scheme 2). Figure 3 shows representative kinetics for the reaction of **2** with 2-

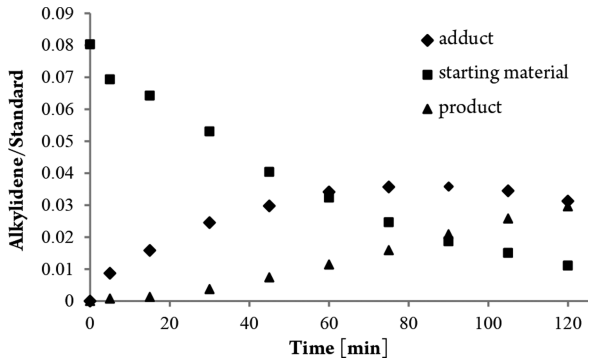

Figure 3. Reaction kinetics for the CM of catalyst **2** with 2-methoxystyrene.

methoxystyrene; the kinetics for all other complexes are summarized in Figures S36−S69, SI

$$[C] = [A]_0 \cdot \left(1 - \frac{k_b \cdot e^{-k_a t} - k_a \cdot e^{-k_b t}}{k_b - k_a}\right) \quad (3)$$

$$[C] = [A]_0 \cdot (1 - e^{-k_a t}) \qquad k_b \gg k_a \quad (4)$$

$$[C] = [A]_0 \cdot (1 - e^{-k_b t}) \qquad k_a \gg k_b \quad (5)$$

Values of k_a were determined directly from the first-order decrease in catalyst concentration (Figures S36−69, SI), and those for k_b were obtained via numerical calculation from eqs 3 and 5,[53,54] which were used to fit the concentration profiles (Figure 3, Figures S17−S34, SI). These describe the concentration profiles of a product [C] formed via two consecutive, irreversible reactions in which either $k_b \gg k_a$ or $k_a \gg k_b$ (Table 1, Table S1, SI). Except for **10** ($R^2 = 0.89$) and **6** ($R^2 = 0.79$), all other R^2 values were 0.98−0.99, see SI. All values were measured in triplicate for each catalyst (Table 1).

Gibbs free activation energies at 303 K, $\Delta G^{\ddagger}_{303}$ (Table 1), for adduct formation were determined by measuring k_a at different temperatures and by calculating the entropy and enthalpy according to the Eyring equation (Table 1, Table S3, SI).[55,56] They describe the cumulative barriers from the parent 16-electron complex to the adduct according to either an associative or a dissociative mechanism as outlined in Scheme 1. By contrast, the above-discussed $\Delta G^{\ddagger}_{Tc}$ for complexes **1**−**5** (vide supra) describes the *dissociative* process of a thermally induced triflate abstraction from the 16-electron progenitor in the *absence* of substrate to yield the cationic complex (Scheme 1, top), while for complexes **6** and **7** it describes again the *associative* reaction of the 16-electron progenitor with triflate, followed by triflate-induced release of another triflate and reformation of the starting complex (Scheme 1, bottom).

In view of the proposed associate mechanism it is not surprising that for complexes **6** and **7** $\Delta G^{\ddagger}_{303}$ and $\Delta G^{\ddagger}_{Tc}$ are almost identical. The small differences can be attributed to the different substrates (triflate vs 2-methoxystyrene). It has to be stressed that in a polar solvent (1,2-dichlorobenzene-d_4) complexes **6** and **7** must indeed both be considered cationic as suggested by the chemical shifts of the triflate anions in the ^{19}F NMR at $\delta = -77.80$ ppm, which in comparison to the chemical shift in TBAT at $\delta = -77.20$ ppm indicate the existence of free triflate (Figure S5, SI). Even in the solid state, the triflate in **6** is only weakly bound to the metal as indicated by the comparably long Mo−O distance (216.1(4) pm).[11] Surprisingly, the Gibbs free activation energy of **9** bearing a coordinating solvent ($\Delta G^{\ddagger}_{303}$ = 80.8 kJ·mol^{-1}) was very comparable to that of catalysts **1**−**5** bearing two triflate ligands. Thus, the $\Delta G^{\ddagger}_{303}$ value of this cationic Mo catalyst must be governed by the dissociation of the coordinated solvent, which stabilizes the complex.

For the bistriflate complexes **1**−**3**, $k_a > k_b$ applied. In these complexes, the rate-determining step is the CM, which is in line with DFT investigations of **2**, where formation of the metallacyclobutane is the rate-determining reaction step and coordination of the substrate has a lower (free) energy barrier.

By contrast, for the bistriflate complexes **4** and **5** $k_b > k_a$ applied. There, coordination of the substrate is the rate-determining step and eq 4 applies. Compared to **1**−**5**, the reactive intermediates of the monoalkoxide monotriflate complexes **6** and **7** were short lived but detectable via NMR at low temperatures (0 or −20 °C). In fact, it could be shown that at both temperatures $k_b > k_a$ and in both complexes, coordination of substrate is the rate-determining step while CM proceeds fast. Table 1 summarizes the values for k_a and k_b.

Table 1. Rate Constants, k_a and k_b, for the Reaction of Catalysts 1−7, 9, and 10 with 2-Methoxystyrene at 30 °C As Determined by ^{1}H NMR Spectroscopy

cat.	T_c [°C]	$\Delta G^{\ddagger}_{Tc}$ [kJ·mol^{-1}]	k_a [L·mol^{-1}·min^{-1}]	k_b [L·mol^{-1}· min^{-1}]	T [°C]	$\Delta G^{\ddagger}_{303}$ [kJ·mol^{-1}]	$\Delta H^{\ddagger}$ [kJ·mol^{-1}·K^{-1}]	$\Delta S^{\ddagger}$[J·mol^{-1}·K^{-1}]
1	100 ± 1[b]	69 ± 0.2[e]	0.164 ± 0.006[a]	0.05 ± 0.001[f]	30	78.6 ± 0.1[a]	62.2 ± 2.5	−54.5 ± 8.4
	90 ± 1[d]							
2	85 ± 1[b]	67 ± 0.2	0.092 ± 0.002[a]	0.05 ± 0.001	30	80.7 ± 0.2[a]	65.6 ± 6.8	−50.0 ± 22.0
3	−3 ± 1[c]	51 ± 0.2	0.161 ± 0.004[b]	0.138 ± 0.011	30	78.3 ± 0.1[c]	92.3 ± 5.3	46.1 ± 17.5
4	−30 ± 1[c]	46 ± 0.2	0.115 ± 0.032[b]	0.356 ± 0.028	30	80.1 ± 0.1[c]	55.0 ± 6.0	−82.8 ± 19.9
5	79 ± 1[a]	66 ± 0.2	0.142 ± 0.037[a]	0.513 ± 0.09	30	78.3 ± 0.1[a]	68.1 ± 5.4	−33.8 ± 18.2
6	82 ± 1[b,d]	69 ± 0.2	1.016 ± 0.155[a]		30	74.1 ± 0.2[a]	51.9 ± 1.5	−73.3 ± 4.6
6			0.11	0.494 ± 0.086	0			
7	82 ± 1[b,d]	69 ± 0.2	2.244 ± 0.326[a]		30	71.7 ± 1.0[a]	49.6 ± 10.0	−72.8 ± 36.5
7			0.038	0.438 ± 0.081	−20			
9			0.085 ± 0.035[a]	0.063 ± 0.002[f]	30	80.8 ± 0.1[a]	13.4 ± 4.5	−222.5 ± 15.0
10			1.0[c]		−10	69.5 ± 0.5[c,g]	27.8 ± 2.7	−137.4 ± 10.5
10			0.38	0.1 ± 0.006[f]	−30			

[a]In $ClCD_2CD_2Cl$. [b]1,2-Dichlorobenzene-d_4.[33] [c]In CD_2Cl_2. [d]With 1 equiv of TBAT. [e]On the basis of the T_c of 100 °C in the absence of additional triflate. [f]Equation 5 for $k_a \gg k_b$ was used. [g]$\Delta G^{\ddagger}_{263}$.

DOI: 10.1021/jacs.9b02092
J. Am. Chem. Soc. 2019, 141, 8264−8276

For the cationic, solvent-stabilized catalyst **9**, again a reactive 16-electron intermediate was observed by ^{1}H NMR ($k_a > k_b$, Table 1, Figures S31−S32, SI) with 2-methoxystyrene coordinated to the metal and coordinated acetonitrile. Clearly, in **9** CM represents the rate-determining step ($k_a > k_b$, Scheme 2, Table 1). Notably, variable-temperature ^{1}H NMR measurements of **9** carried out in 1,2-dichloroethane-d_4 up to 65 °C revealed persistent coordination of acetonitrile to the metal; no free CH_3CN was observed (Figure S35, SI). This is in line with DFT studies, where the formed adduct clearly shows acetonitrile coordination (Figure S131, SI). Moreover, the calculated adduct of **9** is by ∼25−30 kJ·mol^{-1} more stable than the analogous species of **2** (**9$_1$**: ΔE_{rel} = −2.8 kJ·mol^{-1}, ΔG_{303} = 29.2 kJ·mol^{-1}. **2$_1$**: ΔE_{rel} = 19.2·kJ·mol^{-1}, ΔG_{303} = 52.6 kJ) mol^{-1}, and the dissociation of solvent in **9** has a significantly higher barrier ($\Delta E_{rel}^{\ddagger}$ = 38.0 kJ·mol^{-1}/$\Delta G^{\ddagger}_{303}$ = 36.6 kJ·mol^{-1}) compared to dissociation of the second triflate in **2** ($\Delta E_{rel}^{\ddagger}$ = 12.9 kJ·mol^{-1}/ $\Delta G^{\ddagger}_{303}$ = 5.9 kJ·mol^{-1}) (see also Figure S132, SI). Thus, substrate must coordinate first; then the solvent can dissociate, at least at 30 °C. This again confirms the proposed associative mechanism. Preliminary studies suggest a low energy barrier ($\Delta E_{rel}^{\ddagger}$) for the coordination of 2-methoxystyrene at larger distances (between 3.7 and 3.8 Å) to Mo for **9** than found for **2**. In line with that, for the solvent-free cationic complex **10**, coordination of the substrate is fast too, and the subsequent CM is again the rate-determining step, even at −30 °C.

Most important, the value of $\Delta S^{\ddagger}$ provides unambiguous information about the molecularity of the rate-determining step in a reaction. Positive $\Delta S^{\ddagger}$ values suggest that entropy increases in the transition state and are indicative of a *dissociative* mechanism, in which the triflate in the activated complex is either only loosely bound to or even fully dissociated from the metal. Negative values for $\Delta S^{\ddagger}$ indicate that entropy decreases at the transition state. Negative $\Delta S^{\ddagger}$ values were observed for complexes **1**, **2**, and **4**−**10**, thus pointing toward an *associative* mechanism in which two reaction partners form a single activated complex from which triflate then dissociates forming an ion pair. In fact, calculations suggest that triflate sticks to the metal in a distance around 4−5 Å forming an ion pair. We observed a lower energy and free energy for these ion pairs in our calculations, which indicate that it is indeed energetically favorable to keep triflate "nearby". However, we were not able to reliably determine the "correct", i.e., most favorable, position of the triflate because it is hard, if not impossible, to comprehensively sample the complete phase space. We therefore only tested certain positions of the triflate and picked the one that gave the lowest energy. Overall, the electrostatic influence of triflate is rather consistent; it lowers the relative electronic energy by around 50 kJ·mol^{-1} (vide infra). The extremely high negative values for $\Delta S^{\ddagger}$ of both **9** and **10** ($\Delta S^{\ddagger}$ = −222.5 and −137.4 J·mol^{-1}·K^{-1}, respectively) clearly point toward an associative reaction mechanism, which seems to be particularly favored in electron-deficient cationic complexes that have the lowest propensity to release any ligand.

In contrast to all other complexes investigated, catalyst **3** had a positive $\Delta S^{\ddagger}$ value and deserves special consideration. The positive $\Delta S^{\ddagger}$ value of **3** can only be understood together with its T_c value of −3 °C. At 30 °C in solution, the transition state for **3** with 2-methoxystyrene binding to the metal must be such that OTf dissociates to a maximum extent, thereby increasing entropy. This is in contrast to **4**, which has a T_c of −30 °C (CH_2Cl_2, Figure S1, SI). At 30 °C, OTf is already fully dissociated even in the absence of substrate and entropy decreases via associative adduct formation as also found for **1**, **2**, and **5**−**7**.

Subtle differences in $\Delta G^{\ddagger}_{303}$ also reflect the influence of the NHC ligand on triflate dissociation. Thus, for complexes **1** and **3** bearing the 1,3-dimesitylimidazolidin-2-ylidene ($IMesH_2$) ligand, the $\Delta G^{\ddagger}_{303}$ values were around 78 kJ·mol^{-1}, while the corresponding analogues **2** and **4** based on the 1,3-dimesitylimidazol-2-ylidene (IMes) ligand showed a slightly higher energy barrier around 80 kJ·mol^{-1}. This finding correlates with the stronger electron-donor propensity of the $IMesH_2$ ligand compared to the IMes ligand, which is also reflected by the differences in their pK_a values (21.3 vs 20.8)[57] and Tolman electronic parameters (2052.0 vs 2050.8 cm^{-1}),[58] respectively. Interestingly, replacement of the 2,6-Me_2- or 3,5-Me_2-phenylimido ligand in **2** and **4**, respectively, by the 2-tBu-phenylimido ligand (catalyst **5**) resulted in no significant differences in the $\Delta G^{\ddagger}_{303}$ values. However, exchange of one triflate ligand by a pentafluorophenoxide ligand further reduces $\Delta G^{\ddagger}_{303}$ in **6** and **7** to 74.1 and 71.7 kJ·mol^{-1}, respectively. This decrease in $\Delta G^{\ddagger}_{303}$ is in line with the reported higher productivity and activity of Mo−imido alkylidene monoalkoxy monotriflate NHC complexes compared to their bistriflate progenitors.[27,29,31,33,38]

Quantum Chemical Investigation of the Reaction Mechanism for the CM of 2 To Form 2a. For the investigation of the reaction mechanism, the X-ray crystal structures of **2** and **2a** served as starting structures. To reduce stereochemical complexity, the alkylidene moiety was modified to neopentylidene to determine the reaction coordinates involved. All reported electronic energies were calculated with the BP86 density functional,[59,60] the def2-TZVP basis set,[61] empirical dispersion corrections of the Grimme type,[62,63] and implicit solvent interactions modeled with the conductor-like screening model (COSMO) with ε = 9.0 to account for 1,2-dichloroethane[64] as single points on the fully optimized BP86/def2-SV(P)[61]/COSMO(ε = 9.0) structures. To account for the potential influence of dissociated triflate on the cationic structures, the effect of triflate at various positions was tested. It has a minor influence on the structure and the energies between the conformers with both triflates present differ typically around 10−15 kJ·mol^{-1}. In the studied case, the cationic catalyst and the triflate form an ion pair requiring explicit treatment of the second triflate, which lowers the relative energies of each species by ∼50 kJ·mol^{-1} and which was necessary to obtain energies comparable to experiment. At the same time this makes a reliable assignment of free energies very challenging because it would require a complete reoptimization of each cationic structure and transition state of **2** in the presence of the second triflate and an adequate accounting for its conformational degrees of freedom. However, if we assume that in such an ion pair the translational entropy of the triflate is negligible and its rotation is significantly hindered due to its electrostatic interaction with the cationic catalyst, we do not have to account for these entropic contributions of the triflate. Rather, we could apply the quasi-harmonic rigid rotator/harmonic oscillator approximation to calculate thermal corrections and entropic contributions of the whole electrostatic encounter complex (ion pair). Of course, this is an approximation, but it is deemed reasonable, even more so since rotational and translational degrees of freedom are expected to be quenched in the solution phase.[65] Thermal and entropic corrections to the electronic energies were obtained at the BP86/def2-SV(P)[61]/COSMO(ε = 9.0) level.

DOI: 10.1021/jacs.9b02092
J. Am. Chem. Soc. 2019, 141, 8264−8276

Scheme 3. Detailed Associative Reaction Mechanism of 2 To Form 2a[a]

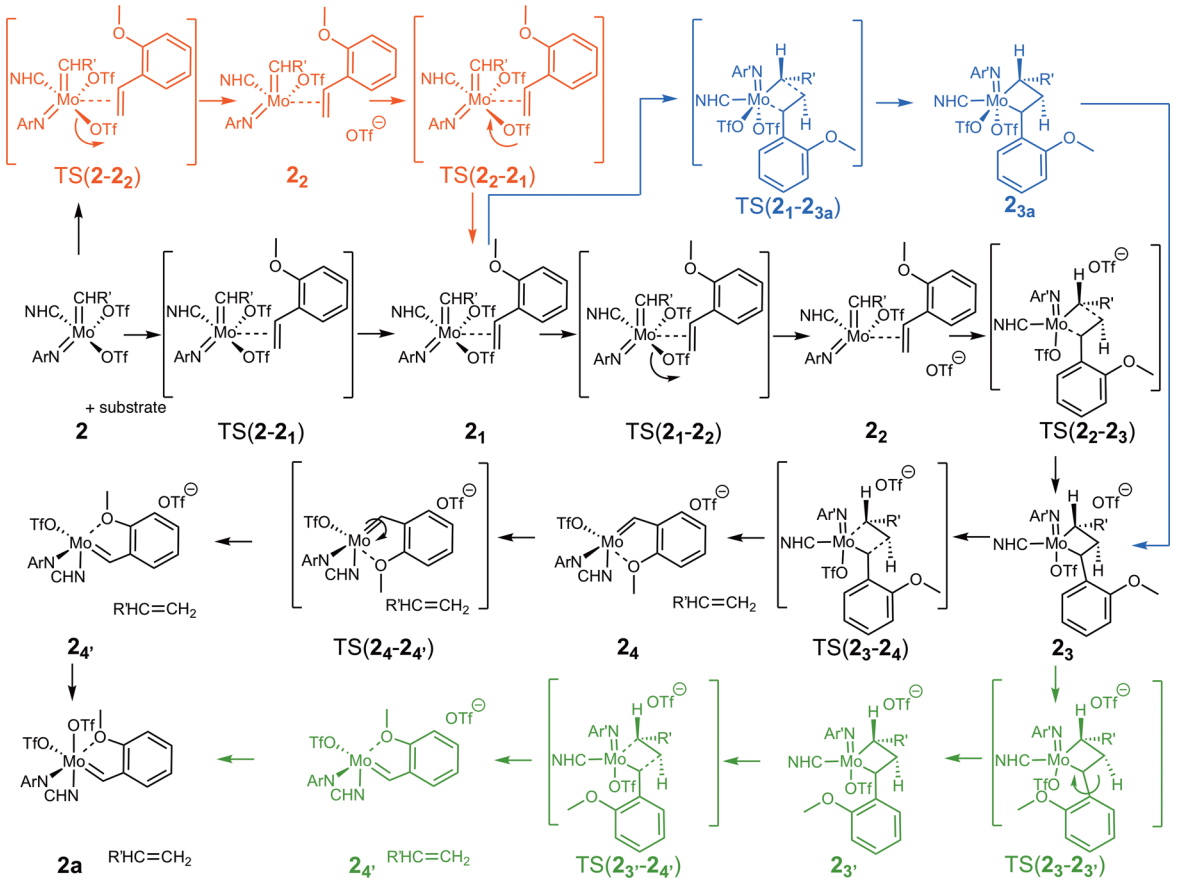

[a]Black: Main proposed reaction pathway. Red: Alternative reassociative activation mechanism with fast recombination to adduct $\mathbf{2_1}$. Blue: Alternative ring-closing mechanism with both triflates coordinated. Green: Alternative ring-opening mechanism. Please note that **2a** crystallizes in a chiral space group containing both enantiomers, and calculations were done for the enantiomer depicted.

To calculate reliable reaction free energies at 303 K, the following measures were taken: Obtained vibrational modes were scaled with a factor of 1.0207,[66] low frequencies below 50 cm^{-1} were shifted to 50 cm^{-1} to minimize artifacts due to the harmonic-oscillator approximation, and conversion of the standard state from 1 atm to 1 mol L^{-1} was accounted for.

The complete reaction mechanism from **2** to **2a** is depicted in Scheme 3, and the corresponding relative free energies ΔG_{303} are shown in Figure 4; relative electronic energies ΔE_{rel} are listed in italic. Only the anti conformation of the alkylidene in **2** was considered (see Figure S104, SI), pointing away from the *N*-aryl as opposed to pointing toward the *N*-aryl in the syn isomer, because previous studies found a preference for the anti isomer.[26,35] Also, the adduct structure was by ~20 kJ·mol^{-1} more stable if the alkylidene adopted an anti conformation.

As already outlined, in the predominant mechanism, **2** coordinates the substrate in an *associative* pathway to form the neutral adduct $\mathbf{2_1}$ (see Figure 6). Adduct $\mathbf{2_1}$ has a relative stability of 19.2 kJ·mol^{-1} (ΔG_{303} = 52.6 kJ·mol^{-1}), passing a transition state TS($\mathbf{2-2_1}$) with a free energy barrier of $\Delta G^{\ddagger}_{303}$ = 72.8 kJ·mol^{-1} ($\Delta E^{\ddagger}_{rel}$ = 42.8 kJ·mol^{-1}) as depicted in Figure S115, SI. Although there is more space to coordinate 2-methoxystyrene trans to the alkylidene group, all attempts to converge such a conformation failed. Instead, coordination of 2-methoxystyrene trans to NHC under deformation of the Mo coordination sphere was found to be the stable species as shown in Figure 6. The depicted conformer was the only stable

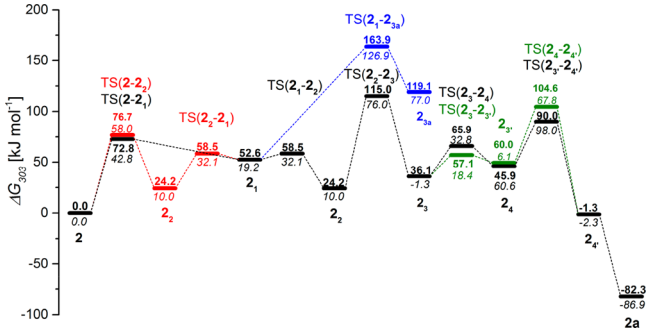

Figure 4. Detailed proposed reaction mechanism for the CM of **2** to form **2a**: (black) predominant reaction pathway with an associative initiation reaction; (red) alternative reassociative reaction mechanism; (blue) alternative ring-closing mechanism with both triflates coordinated; (green) alternative ring-opening mechanism. Relative Gibbs free energies (in kJ·mol^{-1}) were obtained with BP86/def2-TZVP/D3 using 1,2-dichloroethane as implicit solvent (ε = 9). Relative electronic energies are listed in italic.

structure that could be converged; all other orientations of 2-methoxystyrene did not converge to a stable adduct structure. In the obtained conformer the trigonal pyramidal coordination sphere of the free catalyst is modified; the triflate−Mo−alkylidene angle increases, so that a square-pyramidal coordination sphere is formed in the adduct bringing the two phenyl rings in closer vicinity and allowing for some $\pi-\pi$ stacking. The

DOI: 10.1021/jacs.9b02092
J. Am. Chem. Soc. 2019, 141, 8264−8276

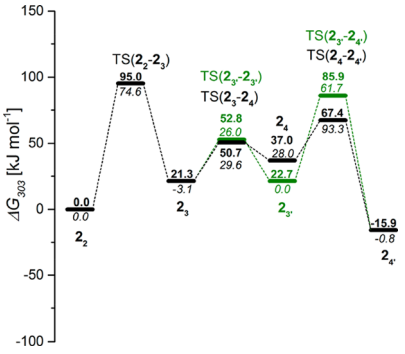

Figure 5. Detailed proposed reaction mechanism for the CM of **2** starting from the catalytically active cationic species $\mathbf{2_2}$ in the absence of the decoordinated triflate: (black) predominant reaction pathway; (green) alternative ring-opening reaction mechanism. Energy of $\mathbf{2_2}$ was arbitrarily set to zero. Relative Gibbs free energies in (kJ·mol^{-1}) were obtained with BP86/def2-TZVP/D3 using 1,2-dichloroethane as implicit solvent (ε = 9). Relative electronic energies are given in italic.

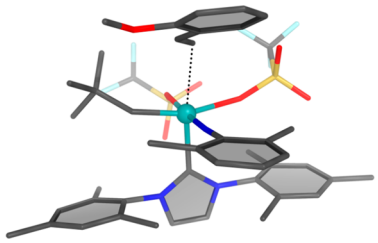

Figure 6. Quantum chemically determined adduct structure $\mathbf{2_1}$. There 2-methoxystyrene is coordinated trans to the NHC.

calculated distance of the Mo to the β-carbon of the vinyl group is 2.5 Å, while it is 3.1 Å for the α-carbon. Additionally, the two hydrogen atoms at the β-carbon are moved out of the planar arrangement, suggesting η^1-coordination to Mo through the β-carbon. Alternatively, $\mathbf{2_1}$ may be formed in a reassociative pathway (TS($\mathbf{2}$–$\mathbf{2_2}$)) as depicted in red in Scheme 3 and Figure 4, where a cationic species $\mathbf{2_2}$ is formed under initial dissociation of triflate in the first reaction step, which then undergoes fast recombination with triflate to form the neutral adduct $\mathbf{2_1}$ (see Figures S107 and S116). While the activation energy barrier of this reassociative mechanism is 58.0 kJ·mol^{-1}, somewhat higher for the rate-determining step than for the associative pathway, the activation free energy barriers are quite similar, $\Delta G^{\ddagger}_{303}$ = 76.8 kJ·mol^{-1} (reassociative) vs $\Delta G^{\ddagger}_{303}$ = 72.8 kJ·mol^{-1} (associative), which results in an energy difference of the two transition states of $\Delta\Delta E_{rel} \approx 16$ kJ·mol^{-1} and a $\Delta\Delta G^{\ddagger}_{303} \approx 4$ kJ·mol^{-1}. To further elucidate this finding, we performed BP86/D3 as well as domain-based local pair-natural orbital coupled cluster (DLPNO-CCSD(T))[67,68] single-point calculations on the converged TS structures, which revealed a $\Delta\Delta E_{rel}$ of ~40 (BP86/D3) and ~44 kJ·mol^{-1} (DLPNO-CCSD(T)) in favor of the associative pathway in the gas phase. Thus, the reassociative mechanism benefits from solvent stabilization, which may open a route for further catalyst development. As solvent effects are only modeled by the standard conductor-like screening model, it may affect the accuracy of the description and the energies obtained. Still, based on the calculated results the reassociative mechanism may not be ruled out. A third potential reaction mechanism comprises the (thermally induced) dissociation of triflate forming the 14-electron cationic catalyst species. While the activation energy barrier is somewhat higher than for the two previously discussed mechanisms ($\Delta E^{\ddagger}$ = 71.5 kJ·mol^{-1}), the activation free energy barrier is $\Delta G^{\ddagger}_{303}$ = 71.4 kJ·mol^{-1}, even slightly lower than for the associative pathway. However, this TS benefits even more from solvent stabilization with $\Delta\Delta E_{rel}$ of ~74 (BP86/D3) and ~65 kJ·mol^{-1} (DLPNO–CCSD(T)) in the gas phase, and again the approximative description of the solvent in the calculations may compromise the accuracy of the calculated (free) energies. Moreover, here, the complex formed between the decoordinated solvent and the cationic catalyst is energetically not favorable. In fact, with our computational methodology we find that the ion pair is by 5 kJ·mol^{-1} less stable in free energy than the TS, which may point to inadequacies in the calculation of thermal and entropic corrections or insufficient sampling of the triflate space. On the basis of these considerations, we wish to exclude this reaction pathway, since it is not in line with experimental findings, which did not reveal formation of any free triflate.

Once the adduct $\mathbf{2_1}$ is formed, one triflate can dissociate with a relative energy of the TS($\mathbf{2_1}$–$\mathbf{2_2}$) of 32.1 kJ·mol^{-1} and a relative free energy of 58.5 kJ·mol^{-1} (barrier height $\Delta E^{\ddagger}_{rel}$ = 12.9 kJ·mol^{-1} and $\Delta G^{\ddagger}_{303}$ = 5.9 kJ·mol^{-1}) forming a stable cationic intermediate $\mathbf{2_2}$ (E_{rel} = 10.0 kJ·mol^{-1} and ΔG_{303} = 24.2 kJ·mol^{-1}). ^{19}F NMR spectroscopy (Figure S13) suggests a mixture of the two species, which is reasonable considering the relative energies of the two species $\mathbf{2_1}$ and $\mathbf{2_2}$. The cationic intermediate $\mathbf{2_2}$ is proposed to be the reactive species and can undergo ring closing, surpassing a transition state TS($\mathbf{2_2}$–$\mathbf{2_3}$) with a relative energy of 76.0 kJ·mol^{-1} (ΔG_{303} = 115.0 kJ·mol^{-1}) and a barrier height of $\Delta E^{\ddagger}_{rel}$ = 66.0 kJ·mol^{-1} and $\Delta G^{\ddagger}_{303}$ = 90.8 kJ·mol^{-1} (see Figure 7) to form the metallacyclobutane $\mathbf{2_3}$ (Figure S109, SI).

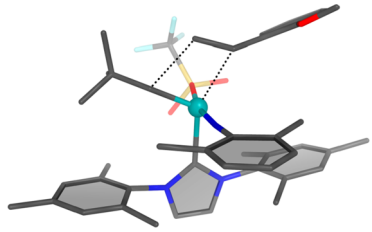

Figure 7. Optimized geometry of the transition state for ring-closing TS($\mathbf{2_2}$–$\mathbf{2_3}$). 2-Methoxystyrene is rotated such that the two alkylidene groups are almost parallel.

Alternatively, the neutral adduct $\mathbf{2_1}$ may directly undergo ring closing to form the neutral metallacyclobutane $\mathbf{2_{3a}}$, in which both triflates are fully coordinated to Mo. However, the corresponding transition state TS($\mathbf{2_1}$–$\mathbf{2_{3a}}$) (Figure S119, SI) is with ΔE_{rel} = 126.9 kJ·mol^{-1} and ΔG_{303} = 163.9 kJ·mol^{-1} (barrier height $\Delta E^{\ddagger}_{rel}$ = 107.7 kJ·mol^{-1} and $\Delta G^{\ddagger}_{303}$ = 111.3 kJ·mol^{-1}) rather high in energy, which renders this pathway quite unlikely. Likewise, the neutral metallacyclobutane $\mathbf{2_{3a}}$ (Figure S110, SI) has also a rather high relative energy of 77.0 kJ·mol^{-1} and ΔG_{303} = 119.1 kJ·mol^{-1}, whereas the cationic metallacyclobutane $\mathbf{2_3}$ is rather stable (ΔE_{rel} = −1.3 kJ·mol^{-1} and ΔG_{303} = 36.1 kJ·mol^{-1}).

To form the transition state for ring closing, the NHC–Mo–alkylidene angle increases and the 2-methoxystyrene is rotating anticlockwise, so the two alkylidene units are nearly parallel to each other (Figure 7). The conformation of the adduct $\mathbf{2_1}$, which was found to be the only stable one, also dictates the conformation of the metallacyclobutane $\mathbf{2_3}$. For cycloreversion and product formation, the 2-methoxyphenyl moiety has to

DOI: 10.1021/jacs.9b02092
J. Am. Chem. Soc. 2019, 141, 8264–8276

rotate by ∼180° to allow chelate formation as found in the crystal structure of **2a**. Two potential pathways are possible: The first entails cycloreversion of $\mathbf{2_3}$ to form $\mathbf{2_4}$ via a transition state for ring-opening TS($\mathbf{2_3}$-$\mathbf{2_4}$) with a relative energy of E_{rel} = 32.8 kJ·mol^{-1} and ΔG_{303} = 65.9 kJ·mol^{-1}, while the barrier height amounts to $E_{rel}^{\ddagger}$ = 34.1 kJ·mol^{-1} and $\Delta G^{\ddagger}_{303}$ = 29.8 kJ·mol^{-1} (Figure 8). In the transition state, the NHC−Mo−alkylidene

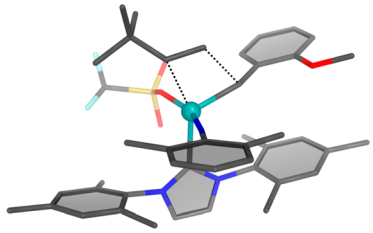

Figure 8. Optimized geometry of the ring-opening transition state TS($\mathbf{2_3}$−$\mathbf{2_4}$).

angle increases to almost 180°. The Mo−C bond weakens and elongates due to the trans effect of NHC, and simultaneously the C−C bond of 2-methoxystyrene weakens, eventually releasing RCH═CH_2. The obtained species $\mathbf{2_4}$ (Figure S113, SI), where the ejected RCH═CH_2 is treated at infinite distance, is only stabilized by entropic effects releasing 20 kJ·mol^{-1} upon formation (ΔG_{303} = 45.9 kJ·mol^{-1}). By rotation of the 2-methoxyphenyl moiety $\mathbf{2_{4'}}$ is obtained (E_{rel} = 2.3 kJ·mol^{-1} and ΔG_{303} = −1.3 kJ·mol^{-1}) (Figure S112, SI). However, due to the bulkiness of the methoxyphenyl group, its reorientation is rather hindered with a high-lying transition state TS($\mathbf{2_4}$−$\mathbf{2_{4'}}$) of ΔE_{rel} = 98.0 kJ·mol^{-1} (ΔG_{303} = 90.0 kJ·mol^{-1}) and a barrier to rotation of $\Delta E_{rel}^{\ddagger}$ = 37.4 kJ·mol^{-1} and $\Delta G^{\ddagger}_{303}$ = 44.1 kJ·mol^{-1} (Figure 9).

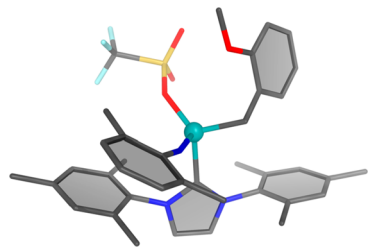

Figure 9. Optimized geometry of the transition state for methoxyphenyl rotation TS($\mathbf{2_4}$−$\mathbf{2_{4'}}$).

The final product **2a** is formed by recombination with the second triflate and shows the lowest relative energy E_{rel} = −86.9 kJ·mol^{-1} (ΔG_{303} = −82.9 kJ·mol^{-1}) of all reaction species.

In an alternative pathway, depicted in green in Scheme 3, Figures 4 and 5, rotation of the 2-methoxyphenyl unit to form the ring conformer $\mathbf{2_{3'}}$ occurs (Figure S111, SI). It has almost the same stability as $\mathbf{2_3}$ in terms of energy (E_{rel} = 6.1 kJ·mol^{-1}) and free energy (ΔG_{303} = 49.3 kJ·mol^{-1}). For this process, a transition state with a relative energy of 18.4 kJ·mol^{-1} (ΔG_{303} = 57.1 kJ·mol^{-1}) and a barrier of rotation of $\Delta E_{rel}^{\ddagger}$ = 19.7 kJ·mol^{-1} ($\Delta G^{\ddagger}_{303}$ = 21.0 kJ·mol^{-1}) was found (Figure S120, SI). This is followed by a transition state for ring opening TS($\mathbf{2_{3'}}$−$\mathbf{2_{4'}}$), for which a relative energy of ΔE_{rel} = 67.8 kJ·mol^{-1} and ΔG_{303} = 104.6 kJ·mol^{-1} (barrier height $\Delta E_{rel}^{\ddagger}$ = 61.7 kJ·mol^{-1} and $\Delta G^{\ddagger}_{303}$ = 55.3 kJ·mol^{-1}) was determined (Figure S122. SI) to form the cationic product $\mathbf{2_{4'}}$, which ultimately undergoes recombination with the second triflate to form the product **2a**. While this reaction pathway is favored in terms of relative electronic energy, entropic effects render this pathway less favorable, making the cycloreversion followed by 2-methoxystyrene rotation the predominant pathway.

Even in the cationic species the triflate stays in proximity to the Mo center; a distance of 4−5 Å is energetically preferred. However, the sampling of the conformational space to find the energy minimum of the triflate turned out to be very challenging. To access the energetic and structural influence of the weakly bound triflate, the cationic species $\mathbf{2_3}$, $\mathbf{2_{3'}}$, $\mathbf{2_4}$, $\mathbf{2_{4'}}$, and the corresponding transition states were (partially) reoptimized with various positions of the free triflate. Of course, this does by no means sample the required phase space; however, results were very consistent. For all structures and transition states, the explicit incorporation decreased the relative energy compared to a triflate at infinite distance to the Mo complex by approximately 50 kJ·mol^{-1} and also decreased free energies, though to a smaller amount. Almost the same extent of stabilization was found in case no dispersion interaction was included in the calculation, suggesting this effect is mainly due to long-range electrostatic stabilization. Incorporation of a weakly bound triflate forms an ion pair in the form of a super molecule and made calculation necessary to obtain the electronic energies as well as free energies that were comparable along the reaction pathway. In case the decoordinated triflate was to be treated at infinite distance to the Mo, energy barriers would have been obtained, which are way too high compared to experiment. However, we could compare the relative reaction energies and barriers of the ion pair with the fully cationic species when starting from the catalytically active species $\mathbf{2_2}$, for which the relative energy was taken as reference and arbitrarily set to zero and the decoordinated triflate was treated at infinite distance.

Calculated relative energies and free energies of the cationic species when starting from $\mathbf{2_2}$ (Figure 5) are consistent with those obtained for the ion pair. Considering the relative energy differences with respect to $\mathbf{2_2}$, both the cationic (in the absence of the second triflate) and the previously discussed reaction path with the second triflate present accounted for as an ion pair complex yield very similar energies (compare Figures 4 and 5). In both cases, the transition state for ring-closing TS($\mathbf{2_2}$−$\mathbf{2_3}$) had a barrier of approximately 75 kJ·mol^{-1} corresponding to an activation free energy of $\Delta G^{\ddagger}_{303}$ = 95 kJ·mol^{-1} (cationic) and $\Delta G^{\ddagger}_{303}$ = 90.8 kJ·mol^{-1} (ion pair complex). The ring-opening mechanism has a low-lying transition state TS($\mathbf{2_3}$-$\mathbf{2_4}$) with a relative energy of ΔE_{rel} = 29.6 kJ·mol^{-1} and a free energy of ΔG_{303} = 50.7 kJ·mol^{-1} (barrier height $\Delta E_{rel}^{\ddagger}$ = 32.7 kJ·mol^{-1} and $\Delta G^{\ddagger}_{303}$ = 29.4 kJ·mol^{-1}) yielding $\mathbf{2_4}$ with a relative energy of ΔE_{rel} = 28.0 kJ·mol^{-1} and ΔG_{303} = 37.0 kJ·mol^{-1} as shown by black bars in Figure 5. Rotation of the 2-methoxyphenyl substituent results in a rather high relative energy of the transitions state TS($\mathbf{2_4}$−$\mathbf{2_{4'}}$) with a barrier height of $\Delta E_{rel}^{\ddagger}$ = 65.3 kJ·mol^{-1}, but entropic and thermal effects decrease this to $\Delta G^{\ddagger}_{303}$ = 30.4 kJ·mol^{-1}. For the resulting species $\mathbf{2_{4'}}$ a relative energy of −0.8 kJ·mol^{-1} is found, whereas ΔG_{303} = −15.9 kJ·mol^{-1}. Similarly, as shown in Figure 5 (green structures), the barrier of rotation for the 2-methoxyphenyl substituent to form $\mathbf{2_{3'}}$ is rather low $\Delta E_{rel}^{\ddagger}$ = 29.1 kJ·mol^{-1} and $\Delta G^{\ddagger}_{303}$ = 31.5 kJ·mol^{-1} compared to $\Delta E_{rel}^{\ddagger}$ = 19.7 kJ·mol^{-1} and $\Delta G^{\ddagger}_{303}$ = 21.0 kJ·mol^{-1} obtained when the second triflate was incorporated in an ion complex pair calculation. The following ring-opening transition state TS($\mathbf{2_{3'}}$−$\mathbf{2_{4'}}$) has a relative energy and a barrier height of 61.7 kJ·mol^{-1} (ΔG_{303} = 85.9 kJ·mol^{-1}) for the fully cationic pathway as indicated by the green bars in Figure 5.

DOI: 10.1021/jacs.9b02092
J. Am. Chem. Soc. 2019, 141, 8264−8276

While this alternative pathway is favored in electronic energy, entropic effects and thermal corrections make it less favorable compared to the former (black bars in Figure 5). Differences in free energy between the ion pair complex and the analogous cationic species, where the decoordinated second triflate is treated at infinite distance, may arise due to insufficient sampling of the triflate space or to an incorrect description of the entropic contributions.

Considering the complete reaction pathway based on the predicted energies as depicted in Scheme 3 and Figures 4 and 5, the predominant mechanism with the lowest relative energies of the transition states comprises the direct formation of the neutral adduct $\mathbf{2}_1$, where the substrate is coordinated to the neutral catalyst. What follows is dissociation of one triflate, a transition state for ring closing, TS($\mathbf{2}_2$–$\mathbf{2}_3$), which has the highest relative energy and is predicted to be the rate-determining step, a transition state for ring opening (cycloreversion), which has a low barrier, and a rotation of the 2-methoxyphenyl substituent, which has a somewhat higher barrier than cycloreversion. Obtained free energies are in line with experimental findings as summarized in Table 1, where a free energy of $\Delta G^{\ddagger}_{303}$ = 80.7 kJ·mol^{-1} is found for the rate-determining associative adduct formation step, whereas calculations predict a value of $\Delta G^{\ddagger}_{303}$ = 72.8 kJ·mol^{-1}. In agreement with experiment, the direct association of the substrate has a significantly lower barrier than the transition state for ring closing and is not rate determining. On the basis of the predicted energies, an alternative reassociative mechanism (shown in red in Figure 4) seems less likely but may not completely be ruled out, especially because it is very similar in free energy to the associative mechanism. By contrast, the alternative neutral ring-closing mechanism (depicted in blue in Figure 4) is energetically less favorable and thus unlikely to occur.

Adduct Stability for Various Substrates. To test the effect of stabilization caused by dispersive π–π stacking interactions between the *N*-aryl group of **2** and the phenyl group of 2-methoxystyrene in $\mathbf{2}_1$, a number of substrates were investigated. Table 2 shows the relative energies with respect to the free catalysts and substrates investigated. When modifying the substrate to 2,2-dimethylpent-4-ene the stability of the adduct decreased by ∼12 kJ·mol^{-1}, suggesting a stabilizing effect of the dispersive π–π stacking interactions. However, even for ethylene, a stable adduct, although energetically less favorable (ΔE_{rel} = 52.2 kJ·mol^{-1}), was found. If, however, *t*-Bu-ethylene was used as a substrate, no stable adduct conformation could be converged. This can be understood by the steric hindrance of the *t*-Bu group, which pushes the substrate away from the Mo center. To further shed light on this, we also tested a hypothetical catalyst, 2-*N*-methyl, in which the Mo(=*N*-aryl) group is replaced by Mo(=*N*–CH_3). The relative stability of the 2-methoxystyrene adduct decreased only marginally by ca. 5 kJ·mol^{-1}. An adduct comparable in stability was also found for 2,2-dimethylpent-4-ene. Remarkably, it is 7 kJ·mol^{-1} more stable than its analogous structure with **2**. Again, the *t*-Bu-ethylene substrate did not yield a stable adduct, while for ethylene a stable adduct was converged. In line with the results for 2,2-dimethylpent-4-ene, this structure was ∼10 kJ·mol^{-1} more stable than the analogous adduct with **2**. Thus, dispersive π–π stacking interactions do play a role in the stability of the adduct $\mathbf{2}_1$, but they are not the only factor that determine the formation of this species. Rather, the deformation of the planar substrate geometry of the ethylene group, which is found for all species, is indicative of an increasing sp^3 character of the carbon that is closest to Mo and η^1-coordination. Bulky substituents at the ethylene, most prominently, *t*-Bu, encounter closed-shell repulsion with the *N*-aryl group and thus increase the Mo–ethylene distance, preventing stabilizing interactions. In the case of 2,2-dimethylpent-4-ene, this destabilizing steric effect is less pronounced because the *t*-Bu group points away from the *N*-aryl group.

Table 2. Relative Stabilities of Various 6-Fold-Coordinated Adducts with 2 and the Modified Catalyst 2-*N*-Methyl[a]

substrate/catalyst	2	2-*N*-methyl
2-methoxystyrene	19.2	24.0
2,2-dimethylpent-4-ene	31.4	24.3
t-Bu-ethylene	not stable	not stable
ethylene	52.2	40.3

[a]Relative electronic energies with respect to the free catalyst and substrate are given in kJ·mol^{-1}.

CONCLUSIONS

In summary, our combined experimental and theoretical studies provide strong evidence for an associative mechanism for both neutral and solvent-stabilized cationic 16-electron Mo imido alkylidene NHC complexes. Such an associative mechanism is in stark contrast to the dissociative pathway that was proposed for solvent-stabilized 16-electron Schrock catalysts, for which tetracoordinate, solvent-free species were proposed to represent the active species. In Mo imido alkylidene NHC complexes, substrate coordinates to the catalyst prior to the release of triflate or solvent. Indeed, the predominant mechanism for neutral 16-electron complexes with the lowest relative energies of the transition states comprises the direct formation of an adduct, in which the substrate is coordinated to the catalyst. A similar result was observed for solvent-stabilized cationic 16-electron complexes; preliminary calculations also suggest a low barrier for substrate coordination and adduct formation. Detailed quantum chemical investigations on **2** to form **2a** are in line with experimental findings, where the rate-determining reaction step is not the initial coordination of substrate to the pentacoordinated (pre-) catalyst but the concomitant CM. Similar to 14-electron Schrock-type catalysts, the quantum chemically determined most stable conformation of $\mathbf{2}_1$ revealed coordination of the substrate trans to the NHC. Generally, in Mo imido alkylidene NHC bistriflate complexes, both adduct formation and CM can be rate determining, depending on the substitution pattern of the (pre-) catalyst. For solvent-stabilized catalyst **9**, a very stable adduct was found and the reaction barrier for acetonitrile dissociation was significantly higher than for triflate dissociation in **2**. Whether this means acetonitrile remains bound to the catalyst or needs to dissociate before CM is speculative and requires further investigation. In Mo imido alkylidene NHC monoalkoxide monotriflate complexes, adduct formation is slower up to a factor of 11 compared to CM and thus represents the rate-determining step. By contrast, both in solvent-stabilized cationic Mo imido alkylidene NHC monotriflate and in solvent-free, cationic 14-electron Mo imido alkylidene NHC monotriflate complexes, CM represents the rate-determining step. In summary, this study provides a clear direction for continuing efforts in catalyst elaboration for these highly promising catalysts for olefin metathesis. This is especially

DOI: 10.1021/jacs.9b02092
J. Am. Chem. Soc. 2019, 141, 8264–8276

true for the design of fully latent, high-T_c precatalysts as well as for both supported and unsupported cationic catalysts.

■ ASSOCIATED CONTENT

Supporting Information

The Supporting Information is available free of charge on the ACS Publications website at DOI: 10.1021/jacs.9b02092.

Crystallographic data for **2a** (CIF)
Crystallographic data for **5** (CIF)
Crystallographic data for **6a** (CIF)
Experimental details for the syntheses and characterization of complexes **5**, **7**−**10**; ^{1}H, ^{13}C, and ^{19}F NMR data; single-crystal X-ray structures of compounds **2a** and **6a**, determination of the coalescence temperatures and NMR kinetic studies; details of the quantum chemical studies of **2** and **9**. CCDC 1841022 (**2a**), CCDC 1836982 (**5**), and CCDC 1841023 (**6a**) contain the supplementary crystallographic data for this paper. These data can be obtained free of charge from The Cambridge Crystallographic Data Centre by The Cambridge Crystallographic Data Centre. (PDF)

■ AUTHOR INFORMATION

Corresponding Authors

*maren.podewitz@uibk.ac.at
*michael.buchmeiser@ipoc.uni-stuttgart.de

ORCID

Maren Podewitz: 0000-0001-7256-1219
Klaus R. Liedl: 0000-0002-0985-2299
Michael R. Buchmeiser: 0000-0001-6472-5156

Notes

The authors declare no competing financial interest.

■ ACKNOWLEDGMENTS

Financial support provided by the Deutsche Forschungsgemeinschaft (DFG, German Research Foundation, project numbers BU 2174/19-1, BU2174/22-1, 358283783-CRC 1333) and XiMo AG, Switzerland, is gratefully acknowledged. M.P. thanks the Austrian Science Fund (FWF) for a generous postdoctoral fellowship (M-2005). Calculations presented in this study have been achieved using the HPC infrastructure LEO of the University of Innsbruck and the Vienna Scientific Cluster (VSC3).

■ REFERENCES

(1) Schrock, R. R. High Oxidation State Multiple Metal-Carbon Bonds. *Chem. Rev.* **2002**, *102*, 145−180.
(2) Schrock, R. R. Multiple Metal−Carbon Bonds for Catalytic Metathesis Reactions (Nobel Lecture). *Angew. Chem., Int. Ed.* **2006**, *45*, 3748−3759.
(3) Grubbs, R. H. Olefin-Metathesis Catalysts for the Preparation of Molecules and Materials (Nobel Lecture). *Angew. Chem., Int. Ed.* **2006**, *45*, 3760−3765.
(4) Vougioukalakis, G. C.; Grubbs, R. H. Ruthenium-Based Heterocyclic Carbene-Coordinated Olefin Metathesis Catalysts. *Chem. Rev.* **2010**, *110*, 1746−1787.
(5) Trnka, T. M.; Grubbs, R. H. The Development of L_2X_2Ru = CHR Olefin Metathesis Catalysts: An Organometallic Success Story. *Acc. Chem. Res.* **2001**, *34*, 18−29.
(6) Schrock, R. R. 133. High Oxidation-State Molybdenum and Tungsten Alkylidyne Complexes. *Acc. Chem. Res.* **1986**, *19*, 342−368.
(7) Schrock, R. R. Recent Advances in High Oxidation State Mo and W Imido Alkylidene Chemistry. *Chem. Rev.* **2009**, *109*, 3211−3226.
(8) Ahmed, T. S.; Grubbs, R. H. Fast-Initiating, Ruthenium-based Catalysts for Improved Activity in Highly E-Selective Cross Metathesis. *J. Am. Chem. Soc.* **2017**, *139*, 1532−1537.
(9) Dornan, P. K.; Wickens, Z. K.; Grubbs, R. H. Tandem Z-Selective Cross-Metathesis/Dihydroxylation: Synthesis of anti-1,2-Diols. *Angew. Chem., Int. Ed.* **2015**, *54*, 7134−7138.
(10) Hartung, J.; Grubbs, R. H. Catalytic, Enantioselective Synthesis of 1,2-anti-Diols by Asymmetric Ring-Opening/Cross-Metathesis. *Angew. Chem., Int. Ed.* **2014**, *53*, 3885−3888.
(11) Herbert, M. B.; Suslick, B. A.; Liu, P.; Zou, L.; Dornan, P. K.; Houk, K. N.; Grubbs, R. H. Cyclometalated Z-Selective Ruthenium Metathesis Catalysts with Modified N-Chelating Groups. *Organometallics* **2015**, *34*, 2858−2869.
(12) Luo, S.-X.; Cannon, J. S.; Taylor, B. L. H.; Engle, K. M.; Houk, K. N.; Grubbs, R. H. Z-Selective Cross-Metathesis and Homodimerization of 3E-1,3-Dienes: Reaction Optimization, Computational Analysis, and Synthetic Applications. *J. Am. Chem. Soc.* **2016**, *138*, 14039−14046.
(13) Mangold, S. L.; O'Leary, D. J.; Grubbs, R. H. Z-Selective Olefin Metathesis on Peptides: Investigation of Side-Chain Influence, Preorganization, and Guidelines in Substrate Selection. *J. Am. Chem. Soc.* **2014**, *136*, 12469−12478.
(14) Koh, M. J.; Nguyen, T. T.; Lam, J. M.; Torker, S.; Hyvl, J.; Schrock, R. R.; Hoveyda, A. Molybdenum Chloride Catalysts for Z-Selective Olefin Metathesis Reactions. *Nature* **2017**, *542*, 80−85.
(15) Lam, J. K.; Zhu, C.; Bukhryakov, K. V.; Müller, P.; Hoveyda, A.; Schrock, R. R. Synthesis and Evaluation of Molybdenum and Tungsten Monoaryloxide Halide Alkylidene Complexes for Z-Selective Cross-Metathesis of Cyclooctene and Z-1,2-Dichloroethylene. *J. Am. Chem. Soc.* **2016**, *138*, 15774−15783.
(16) Peryshkov, D. V.; Schrock, R. R.; Takase, M. K.; Müller, P.; Hoveyda, A. H. Z-Selective Olefin Metathesis Reactions Promoted by Tungsten Oxo Alkylidene Complexes. *J. Am. Chem. Soc.* **2011**, *133*, 20754−20757.
(17) Shen, X.; Nguyen, T. T.; Koh, M. J.; Xu, D.; Speed, A. W. H.; Schrock, R. R.; Hoveyda, A. H. Kinetically E-Selective Macrocyclic Ring-Closing Metathesis. *Nature* **2017**, *541*, 380−387.
(18) Speed, A. W. H.; Mann, T. J.; O'Brien, R. V.; Schrock, R. R.; Hoveyda, A. H. Catalytic Z-Selective Cross-Metathesis in Complex Molecule Synthesis: A Convergent Stereoselective Route to Disorazole C1. *J. Am. Chem. Soc.* **2014**, *136*, 16136−16139.
(19) Townsend, E. M.; Schrock, R. R.; Hoveyda, A. H. Z-Selective Metathesis Homocoupling of 1,3-Dienes by Molybdenum and Tungsten Monoaryloxide Pyrrolide (MAP) Complexes. *J. Am. Chem. Soc.* **2012**, *134*, 11334−11337.
(20) Wang, C.; Haeffner, F.; Schrock, R. R.; Hoveyda, A. H. Molybdenum-Based Complexes with Two Aryloxides and a Pentafluoroimido Ligand: Catalysts for Efficient Z-Selective Synthesis of a Macrocyclic Trisubstituted Alkene by Ring-Closing Metathesis. *Angew. Chem., Int. Ed.* **2013**, *52*, 1939−1943.
(21) Yu, M.; Schrock, R. R.; Hoveyda, A. H. Catalyst-Controlled Stereoselective Olefin Metathesis as a Principal Strategy in Multistep Synthesis Design: A Concise Route to (+)-Neopeltolide. *Angew. Chem., Int. Ed.* **2015**, *54*, 215−220.
(22) Zhang, H.; Yu, E. C.; Torker, S.; Schrock, R. R.; Hoveyda, A. H. Preparation of Macrocyclic Z-Enoates and (E,Z)- or (Z,E)-Dienoates through Catalytic Stereoselective Ring-Closing Metathesis. *J. Am. Chem. Soc.* **2014**, *136*, 16493−16496.
(23) Schrock, R. R. 178. Living Ring-Opening Metathesis Polymerization Catalyzed by Well-Characterized Transition Metal Alkylidene Complexes. *Acc. Chem. Res.* **1990**, *23*, 158−165.
(24) Schrock, R. R. Synthesis of Stereoregular Polymers Through Ring-Opening Metathesis Polymerization. *Acc. Chem. Res.* **2014**, *47*, 2457−2466.
(25) Schrock, R. R. Synthesis of Stereoregular ROMP Polymers Using Molybdenum and Tungsten Imido Alkylidene Initiators. *Dalton Trans.* **2011**, *40*, 7484−7495.
(26) Buchmeiser, M. R.; Sen, S.; Unold, J.; Frey, W. N-Heterocyclic Carbene, High Oxidation State Molybdenum Alkylidene Complexes:

DOI: 10.1021/jacs.9b02092
J. Am. Chem. Soc. 2019, 141, 8264−8276

Functional-Group-Tolerant Cationic Metathesis Catalysts. *Angew. Chem., Int. Ed.* **2014**, *53*, 9384−9388.
(27) Sen, S.; Schowner, R.; Imbrich, D. A.; Frey, W.; Hunger, M.; Buchmeiser, M. R. Neutral and Cationic Molybdenum Imido Alkylidene N-Heterocyclic Carbene Complexes: Reactivity in Selected Olefin Metathesis Reactions and Immobilization on Silica. *Chem. - Eur. J.* **2015**, *21*, 13778−13787.
(28) Schowner, R.; Frey, W.; Buchmeiser, M. R. Cationic Tungsten-Oxo-Alkylidene-N-Heterocyclic Carbene Complexes: Highly Active Olefin Metathesis Catalysts. *J. Am. Chem. Soc.* **2015**, *137*, 6188−6191.
(29) Elser, I.; Frey, W.; Wurst, K.; Buchmeiser, M. R. Molybdenum Imido Alkylidene Complexes Containing N- and C-Chelating N-Heterocyclic Carbenes. *Organometallics* **2016**, *35*, 4106−4111.
(30) Imbrich, D. A.; Elser, I.; Frey, W.; Buchmeiser, M. R. First Neutral and Cationic Tungsten Imido Alkylidene N-Heterocyclic Carbene Complexes. *ChemCatChem* **2017**, *9*, 2996−3002.
(31) Elser, I.; Schowner, R.; Frey, W.; Buchmeiser, M. R. Molybdenum and Tungsten Imido Alkylidene N-Heterocyclic Carbene Catalysts Bearing Cationic Ligands for Use in Biphasic Olefin Metathesis. *Chem. - Eur. J.* **2017**, *23*, 6398−6405.
(32) Herz, K.; Unold, J.; Hänle, J.; Schowner, R.; Sen, S.; Frey, W.; Buchmeiser, M. R. Mechanism of the Regio- and Stereoselective Cyclopolymerization of 1,6-Hepta- and 1,7-Octadiynes by High Oxidation State Molybdenum−Imidoalkylidene N-Heterocyclic Carbene Initiators. *Macromolecules* **2015**, *48*, 4768−4778.
(33) Buchmeiser, M. R.; Sen, S.; Lienert, C.; Widmann, L.; Schowner, R.; Herz, K.; Hauser, P.; Frey, W.; Wang, D. Molybdenum Imido Alkylidene N-Heterocyclic Carbene Complexes: Structure−Productivity Correlations and Mechanistic Insights. *ChemCatChem* **2016**, *8*, 2710−2723.
(34) Buchmeiser, M. R. Recent Advances in the Regio- and Stereospecific Cyclopolymerization of α,ω-Diynes by Tailored Ruthenium Alkylidenes and Molybdenum Imido Alkylidene N-Heterocyclic Carbene Complexes. *Polym. Rev.* **2017**, *57*, 15−30.
(35) Lienert, C.; Frey, W.; Buchmeiser, M. R. Stereospecific Ring-Opening Metathesis Polymerizations with Molybdenum Imido Alkylidenes Containing O-Chelating N-Heterocyclic Carbenes: Influence of syn/anti Interconversion and Polymerization Rates on Polymer Structure. *Macromolecules* **2017**, *50*, 5701−5710.
(36) Pucino, M.; Mougel, V.; Schowner, R.; Fedorov, A.; Buchmeiser, M. R.; Copéret, C. Cationic Silica-Supported N-Heterocyclic Carbene Tungsten Oxo Alkylidene Sites: Highly Active and Stable Catalysts for Olefin Metathesis. *Angew. Chem., Int. Ed.* **2016**, *55*, 4300−4302.
(37) Pucino, M.; Inoue, M.; Gordon, C. P.; Schowner, R.; Stöhr, L.; Sen, S.; Hegedüs, C.; Robé, E.; Tóth, F.; Buchmeiser, M. R.; Copéret, C. Promoting Terminal Olefin Metathesis with Supported Cationic Molybdenum Imido Alkylidene N-Heterocyclic Carbene Catalyst. *Angew. Chem., Int. Ed.* **2018**, *57*, 14566−14569.
(38) Beerhues, J.; Sen, S.; Schowner, R.; Mate Nagy, G.; Wang, D.; Buchmeiser, M. R. Tailored Molybdenum Imido Alkylidene N-Heterocyclic Carbene Complexes as Latent Catalysts for the Polymerization of Dicyclopentadiene. *J. Polym. Sci., Part A: Polym. Chem.* **2017**, *55*, 3028−3033.
(39) Elser, I.; Kordes, B. R.; Frey, W.; Herz, K.; Schowner, R.; Stöhr, L.; Altmann, H. J.; Buchmeiser, M. R. Latent and Air Stable Pre-Catalysts for the Polymerization of Dicyclopentadiene: From Penta- to Hexacoordination in Molybdenum Imido Alkylidene N-Heterocyclic Carbene Complexes. *Chem. - Eur. J.* **2018**, *24*, 12652−12659.
(40) Buchmeiser, M. R.; Sen, S.; Unold, J.; Frey, W. N-Heterocyclic Carbene, High Oxidation State Molybdenum Alkylidene Complexes: Functional-Group-Tolerant Cationic Metathesis Catalysts. *Angew. Chem., Int. Ed.* **2014**, *53*, 9384−9388.
(41) Schrock, R. R.; Lee, J.-K.; O'Dell, R.; Oskam, J. H. Exploring Factors That Determine Cis/Trans Structure and Tacticity in Polymers Prepared by Ring-Opening-Metathesis Polymerization with Initiators of the Type syn- and anti-Mo(NAr)(CHCMe2Ph)(OR)2. Observation of a Temperature-Dependent Cis/Trans Ratio. *Macromolecules* **1995**, *28*, 5933−5940.
(42) Oskam, J. H.; Schrock, R. R. 257. Rotational Isomers of Mo(VI) Alkylidene Complexes and *Cis/Trans* Polymer Structure: Investigations in Ring-Opening Metathesis Polymerization. *J. Am. Chem. Soc.* **1993**, *115*, 11831−11845.
(43) Schrock, R. R.; Hoveyda, A. H. Molybdenum and Tungsten Imido Alkylidene Complexes as Efficient Olefin-Metathesis Catalysts. *Angew. Chem., Int. Ed.* **2003**, *42*, 4592−4633.
(44) Poater, A.; Solans-Monfort, X.; Clot, E.; Coperet, C.; Eisenstein, O. Understanding d(0)-Olefin Metathesis Catalysts: Which Metal, Which Ligands? *J. Am. Chem. Soc.* **2007**, *129*, 8207−8216.
(45) Solans-Monfort, X.; Coperet, C.; Eisenstein, O. Metallacyclobutanes from Schrock-Type d(0) Metal Alkylidene Catalysts: Structural Preferences and Consequences in Alkene Metathesis. *Organometallics* **2015**, *34*, 1668−1680.
(46) Imbrich, D. A.; Frey, W.; Naumann, S.; Buchmeiser, M. R. Application of Imidazolinium Salts and N-Heterocyclic Olefins for the Synthesis of Anionic and Neutral Tungsten Imido Alkylidene Complexes. *Chem. Commun.* **2016**, *52*, 6099−6102.
(47) Eyring, H. The Activated Complex and the Absolute Rate of Chemical Reactions. *Chem. Rev.* **1935**, *17*, 65−77.
(48) Schwab, P.; Grubbs, R. H.; Ziller, J. W. Synthesis and Applications of $RuCl_2(CHR')(PR_3)_2$: The Influence of the Alkylidene Moiety on Metathesis Activity. *J. Am. Chem. Soc.* **1996**, *118*, 100−110.
(49) Zhang, Y.; Santos, A. M.; Herdtweck, E.; Mink, J.; Kuhn, F. E. Organonitrile ligated silver complexes with perfluorinated weakly coordinating anions and their catalytic application for coupling reactions. *New J. Chem.* **2005**, *29*, 366−370.
(50) Seppelt, K. Nichtkoordinierende" Anionen. *Angew. Chem., Int. Ed. Engl.* **1993**, *32*, 1025−1027.
(51) Krossing, I.; Raabe, I. Nichtkoordinierende Anionen - Traum oder Wirklichkeit? Eine Übersicht zu möglichen Kandidaten. *Angew. Chem., Int. Ed.* **2004**, *43*, 2066−2090.
(52) Bochmann, M. Nicht-koordinierende" Anionen: unterschätzte Liganden. *Angew. Chem., Int. Ed. Engl.* **1992**, *31*, 1181−1182.
(53) Petrov, A. I.; Dergachev, V. D. Equivalency of Kinetic Schemes: Causes and an Analysis of Some Model Fitting Algorithms. *Int. J. Chem. Kinet.* **2017**, *49*, 494−505.
(54) Jones, C. T. Determination of the Kinetic Constants of Two Consecutive First-Order Reactions. *Biochem. J.* **1970**, *118*, 810−812.
(55) Eyring, H. The Activated Complex in Chemical Reactions. *J. Chem. Phys.* **1935**, *3*, 107−115.
(56) Evans, M. G.; Polanyi, M. Some Applications of the Transition State Method to the Calculation of Reaction Velocities, Especially in Solution. *Trans. Faraday Soc.* **1935**, *31*, 875−894.
(57) Higgins, E. M.; Sherwood, J. A.; Lindsay, A. G.; Armstrong, J.; Massey, R. S.; Alder, R. W.; O'Donoghue, A. C. pK_as of the Conjugate Acids of N-Heterocyclic Carbenes in Water. *Chem. Commun.* **2011**, *47*, 1559−1561.
(58) Dröge, T.; Glorius, F. The Measure of All Rings—N-Heterocyclic Carbenes. *Angew. Chem., Int. Ed.* **2010**, *49*, 6940−6952.
(59) Becke, A. D. Density-Functional Exchange-Energy Approximation with Correct Asymptotic-Behavior. *Phys. Rev. A: At., Mol., Opt. Phys.* **1988**, *38*, 3098−3100.
(60) Perdew, J. P. Density-Functional Approximation For the Correlation-Energy of the Inhomogeneous Electron-Gas. *Phys. Rev. B: Condens. Matter Mater. Phys.* **1986**, *33*, 8822−8824.
(61) Weigend, F.; Ahlrichs, R. Balanced Basis Sets of Split Valence, Triple Zeta Valence and Quadruple Zeta Valence Quality for H to Rn: Design and Assessment of Accuracy. *Phys. Chem. Chem. Phys.* **2005**, *7*, 3297−3305.
(62) Grimme, S.; Ehrlich, S.; Goerigk, L. Effect of the Damping Function in Dispersion Corrected Density Functional Theory. *J. Comput. Chem.* **2011**, *32*, 1456−1465.
(63) Grimme, S. Semiempirical GGA-Type Density Functional Constructed With a Long-Range Dispersion Correction. *J. Comput. Chem.* **2006**, *27*, 1787−1799.
(64) Klamt, A.; Schüürmann, G. COSMO - A New Approach To Dielectric Screening In Solvents With Explicit Expressions For The

DOI: 10.1021/jacs.9b02092
J. Am. Chem. Soc. 2019, 141, 8264−8276

Screening Energy And Its Gradient. *J. Chem. Soc., Perkin Trans. 2* **1993**, *2*, 799−805.
(65) Dewyer, A. L.; Zimmerman, P. M. Simulated Mechanism for Palladium-Catalyzed, Directed g-Arylation of Piperidine. *ACS Catal.* **2017**, *7*, 5466−5477.
(66) Kesharwani, M. K.; Brauer, B.; Martin, J. M. L. Frequency and Zero-Point Vibrational Energy Scale Factors for Double-Hybrid Density Functionals (and Other Selected Methods): Can Anharmonic Force Fields Be Avoided? *J. Phys. Chem. A* **2015**, *119*, 1701−1714.
(67) Riplinger, C.; Neese, F. An efficient and near linear scaling pair natural orbital based local coupled cluster method. *J. Chem. Phys.* **2013**, *138*, 034106.
(68) Riplinger, C.; Sandhoefer, B.; Hansen, A.; Neese, F. Natural triple excitations in local coupled cluster calculations with pair natural orbitals. *J. Chem. Phys.* **2013**, *139*, 134101.

DOI: 10.1021/jacs.9b02092
J. Am. Chem. Soc. 2019, 141, 8264−8276